*RSC Advances*, 2016, DOI: 10.1039/C6RA22951D

Supplementary information: http://www.rsc.org/suppdata/c6/ra/c6ra22951d/c6ra22951d1.pdf

# Characterization of a Graphene Oxide/Poly(acrylic acid) Nanocomposite by means of Molecular Dynamics Simulations

Kostas Karatasos* and Georgios Kritikos

*Laboratory of Physical Chemistry, Department of Chemical Engineering,*

*Aristotle University of Thessaloniki,*

*54124 Thessaloniki, Greece*

## Abstract

A graphene oxide/poly(acrylic acid) nanocomposite in the melt state was studied by means of fully atomistic molecular dynamics (MD) simulations. The mixture was characterized in a wide temperature range in terms of its thermal behavior and the static and dynamic properties of the polymeric material. In addition, the formation of the intra- and intermolecular hydrogen bonding network was examined in a quantitative manner, and the longevity of the formed hydrogen bonds was estimated. It was found that part of the graphene oxide (GO) flakes formed oligomeric clusters that were dispersed in the polymeric matrix. The presence of GO at the examined composition resulted in a moderate shift of the glass transition temperature of the composite with respect to that of the pristine polymer. The physical adsorption of the polymer chains onto the GO surface was found to be driven mainly by a specific type of hydrogen bonds, while the presence of GO and the temperature change affected the amount of hydrogen bonding among the poly(acrylic acid) (PAA) chains. Polymer dynamics were slowed down appreciably due to the presence of GO, both at the local and at the entire molecular scale. The degree of slowing down for local reorientational motions was examined as a function of the distance from the GO flakes, assessing thus the effect of the physical adsorption and of the effective confinement of polymer chains within the GO clusters.

Elucidation of the microscopic characteristics of the resulted morphology and of the correlation between structure and dynamic response of the components, offers a first step for the interpretation of the observed macroscopic behavior of such nano-hybrid materials.

Tel.: +30-2310-995850; fax: +30-2310-996222; e-mail: karatas@eng.auth.gr

## 1. Introduction

Polymer/graphene-based nanocomposites have lately emerged as promising materials for a wide range of high-end technological applications. Among other uses, they have been found to be of potential use as gas-barrier materials[1-3], as responsive systems for water clean-up[4], as conductive thermoelectric materials[5] and as parts in electronic devices[6], as appropriate materials for the fabrication of fuel cell membranes[7, 8] and as chemical[9] and biological sensors[10].

In the present work we investigate a system comprised by two components that have attracted scientific and industrial interest due to their favourable properties[11-14], namely GO and PAA. Both, GO and PAA are water soluble[15-17], facilitating thus the fabrication of composite materials using environmentally friendly processes, either through a common aqueous dispersion, or by direct melt mixing at elevated temperatures.

The potential of GO/PAA hybrid materials has recently been recognised in studies exploring their use as self-healable materials[18], electroresponsive systems[13], anti-pollutant and cleaning agents[19, 20], electronic components[21] and systems for biomedical uses[22]. Optimization of the physical properties and control of the behavior of such complex systems essentially requires a molecular-level understanding of their structural characteristics, their dynamic response at different time- and length-scales and the physicochemical processes involved in the local thermodynamic environment. On these grounds, molecular simulations can play the role of a detailed technique at the nanoscale, in order to study the microscopic mechanisms that operate at the atomic and/or molecular level and virtually dictate the macroscopic behavior of such materials. Along these lines, we hereby present results from fully atomistic molecular dynamics simulations of a graphene oxide/poly(acrylic acid) mixture.

To our knowledge, this is the first time that a detailed computational study is performed in a GO/PAA system. As a first step we have opted in examining a system without the presence of solvent, mimicking thus a mixture that has been fabricated either by melt-mixing at temperatures above the glass transition, or via an aqueous solution of the two components after complete evaporation of the solvent followed by an annealing procedure at higher temperatures.

Our aim is to obtain new insight on certain aspects of the static, dynamic and thermodynamic behavior of the formed composite, elucidating also details associated

with the interactions between the two components and with the effects of the presence of GO in local and global conformational characteristics of the polymeric material.

## 2. Model description and simulation protocol

The composite system studied was comprised by 7 GO flakes of dimensions 15 Å x 20 Å embedded in a polymer matrix of 30 poly(acrylic acid) atactic chains of 40 monomers each (referred to as 30paa7go henceforth), resulting in a 14.5 w/w% in GO composite. For our study we have chosen to simulate a model with GO content which lies in-between the range of compositions usually examined experimentally for graphene-based polymer nanocomposites[23, 24]. The average size of a PAA chain of the examined molecular weight (~2884 g/mol) as this is determined by the chain radius of gyration (estimated to be approximately 14 Å from our simulations), is comparable to the lateral dimensions of the GO flake. For comparison purposes, we have also simulated a pristine polymer model which served as a reference system for the nanocomposite.

The graphene-oxide flakes were modelled with a carbon to oxygen atom ratio of 5:1 and a hydroxyl to epoxy group ratio of 3:2 approximately, in line with the GO model proposed in refs [25, 26], and terminated with hydrogen atoms as depicted in figure 1.

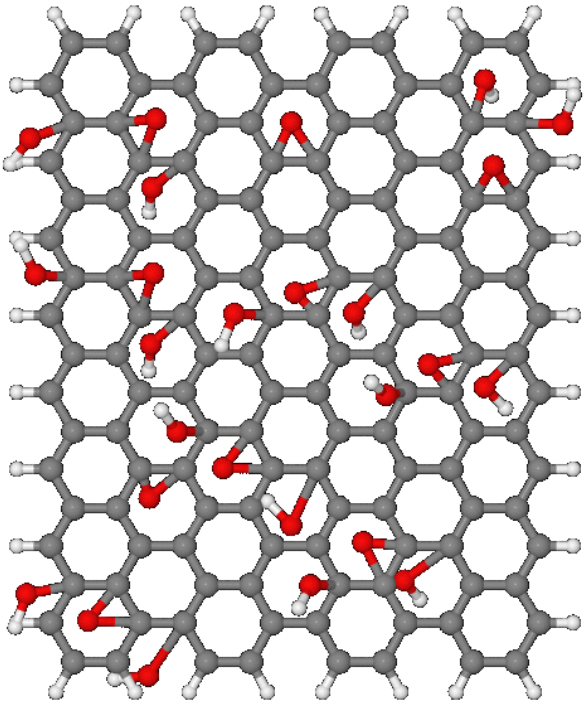

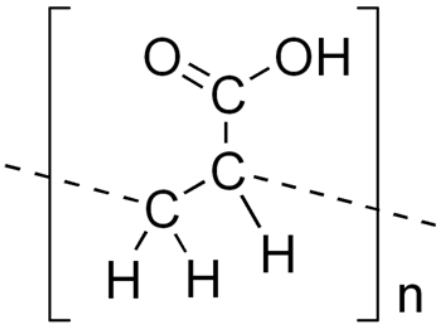

**Figure 1**: Schematic of a GO sheet model (left) and of a PAA monomer (right).

The pristine polymer model was comprised by 40 atactic PAA chains identical to those included in the composite system (referred to as 40paa40). The partial charges for the carbon and oxygen atoms of GO were taken from ref. [25], as well as the atomic interaction parameters which were obtained from the AMBER forcefield[27]. For compatibility purposes and following recent computational works on PAA[28, 29], the respective energetic parameters for the polymer atoms were also based on the AMBER forcefield[27, 30], while the Gasteiger method was used for charge assignment using the AMBER Antechamber module[31].

The initial configurations of the pure polymer model and of the composite were constructed with the Packmol program[32]. To obtain well equilibrated structures the systems were gradually heated by steps of 50 K from ambient temperature up to 650K. At each temperature a combination of energy minimization and MD simulations lasting several tens of ns (depending on temperature) in the isobaric-isothermal ensemble (NPT) were performed. The production trajectories were recorded during the cooling procedure, starting from 650 K down to 300 K. A similar equilibration protocol was also followed at each temperature during the cooling part of the simulation (again with steps of 50 K) with a timestep of 1 fs (using the r-RESPA algorithm for the evaluation of the long-range interactions every two timesteps), a frame saving frequency of 1 ps and at a pressure of 1 bar. The initial structure at each temperature was obtained from the last configuration of the previous temperature. The degree of equilibration at each temperature was determined by the stabilization of characteristic conformational and thermodynamic quantities, such as the total and the partial energies, the density, the radius of gyration of the polymer chains and the spatial arrangement of the molecular species contained in each model.

During the NPT MD runs the temperature control was performed by means of the Langevin method (with a damping coefficient of 5 $ps^{-1}$) and the pressure control by employing the Nose-Hoover Langevin piston method[33] (using a piston period of 0.1 ps and a decay time of 0.05 ps). Electrostatic interactions were taken into account via the particle mesh Ewald (PME) algorithm.[34] All simulations were performed with NAMD 2.11[35] under periodic boundary conditions and with a distance cutoff of 12 Å for non-bonded interactions. All the analysis was performed by custom made routines. Figure 2 portrays the configurations of the composite model before and after the application of the annealing procedure and the equilibration as described above, at

300K. The snapshot of the equilibrated system shows that a number of GO flakes tend to organize into clusters while others remain unpaired within the polymer matrix. The aggregation of GO flakes is similar to the behavior of non-oxidized graphene systems where clusters comprised by 2-3 platelets had been observed[36, 37] .

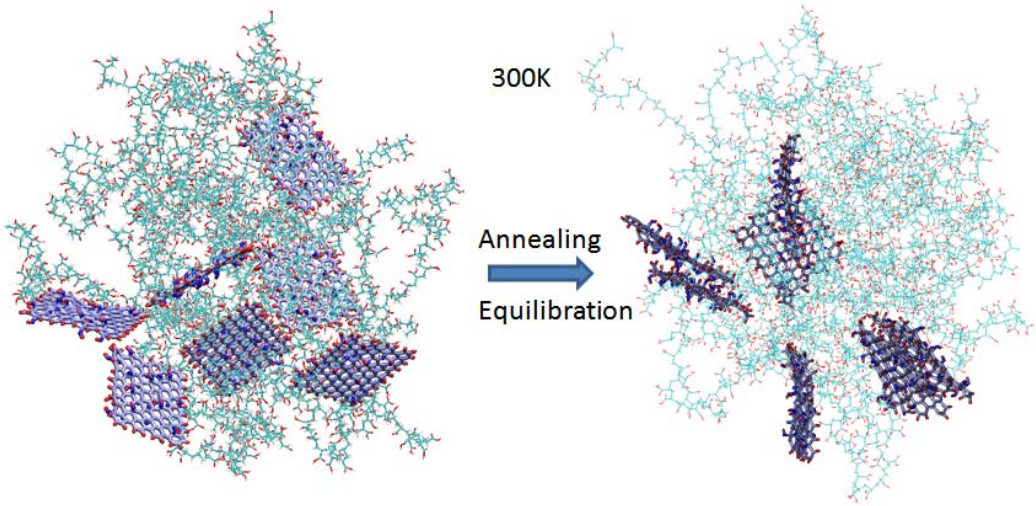


**Figure 2:** Snapshots in unwrapped coordinates of the composite system prior to (left) and after (right) the heating and cooling cycles applied to the system, at 300K.

## 3. Results and discussion

### 3.1. Thermal behavior and chain conformational characteristics

To monitor the thermal response of the examined systems we have followed the temperature dependence of the specific volume.

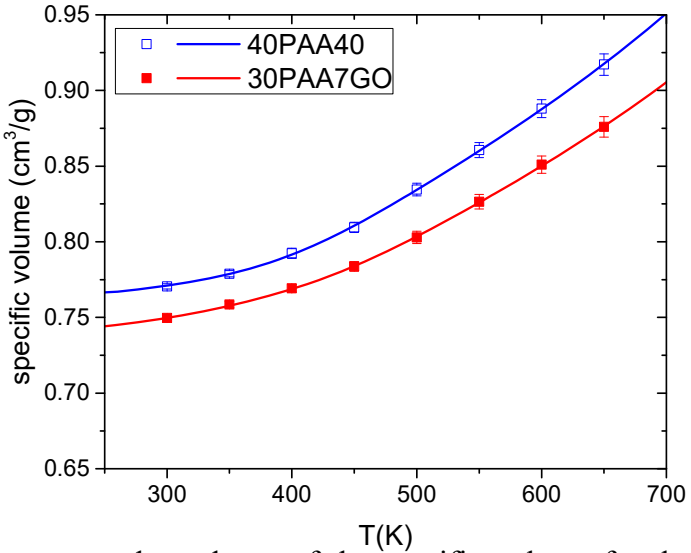


**Figure 3**: Temperature dependence of the specific volume for the pristine polymer and the composite, as obtained during the cooling procedure described in the text

(symbols). The lines through the points denote the result of fitting the data with a modified Sanchez-Lacombe equation (see text).

In figure 3 we depict the temperature dependence of the specific volume for the bulk and the nanocomposite systems. A cursory glance at the data indicates a transition in the rate of change of the specific volume as a function of temperature, implying two distinct regimes. From the low temperature regime (i.e., below 450K) of the simulated bulk PAA model, a thermal coefficient of expansion of 2.13 $\times$ $10^{-4}$ $K^{-1}$ was calculated which compares well with an experimental value[38] of 2.08 $\pm$ 0.04 $\times 10^{-4}$ $K^{-1}$. The aforementioned transition between the two regimes is commonly identified as a glass transition region[39]. In order to estimate the glass transition temperature ($T_g$) in a more accurate manner, we have employed the modified Sanchez-Lacombe equation of state[40]. Although the original lattice fluid model[41] does not predict the characteristic temperature dependence of the density at the glass transition region, the insertion of a sigmoidal temperature dependent pairwise energy was found to describe fairly well the results from simulations and relevant experiments[40]. The estimated glass transition temperatures were 412 $\pm$ 4 K and 450 $\pm$ 10 K for the simulated bulk and the nanocomposite systems respectively. The experimental value for the glass transition temperature of PAA was determined to be 401 K[42] which is reasonably close to the $T_g$ determined from the simulational data as described above. The somewhat higher glass transition temperature value from bulk PAA simulations, can be accounted for if we also take into consideration that the effective cooling rate in simulations is much higher[43] than the usual rate of 10 K/min applied e.g., in differential scanning calorimeter experiments.

The higher $T_g$ value predicted for the composite system is reminiscent of a shift in $T_g$ to higher temperatures with respect to the pure polymer, in functionalized graphene-based nanocomposite materials as this was observed in recent experimental[44] and computational studies[45]. In these works, the increase of the glass transition temperature in the composites was attributed to the presence of functional groups which assisted the physical adsorption of the polymer chains onto the graphene surface. This issue will be discussed in detail in the section 3.3 of the manuscript.

To check whether the presence of GO affected on average the polymer conformational characteristics, we have calculated the characteristic ratio of the PAA chains in the pristine system and in the nanocomposite as depicted in figure 4.

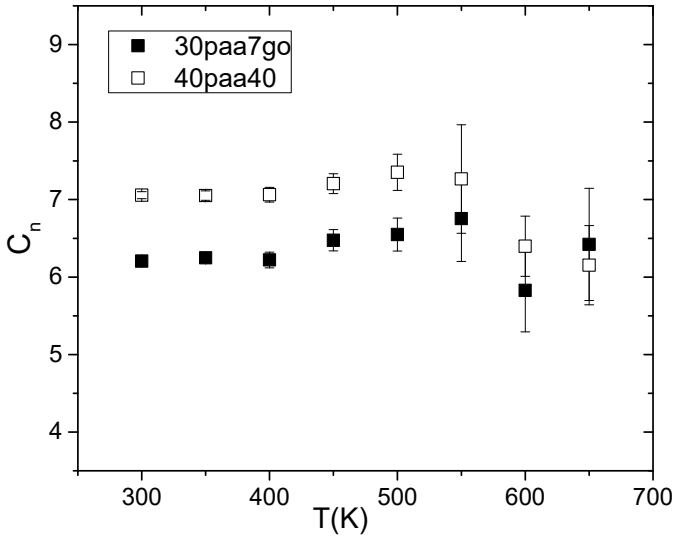


**Figure 4**: Characteristic ratio of the PAA chains in the examined systems

The characteristic ratio is defined as

$$c_n = \frac{\left\langle R^2_{e-e} \right\rangle}{nl^2} \quad (1)$$

where $\left\langle R^2_{e-e} \right\rangle$ corresponds to the mean-square end-to-end distance of the polymer chain, *n* denotes the number of main-chain backbone bonds and *l* is the mean length per skeletal bond. As shown, at all temperatures the ratio remains very close to the value of 6.7 which represents the characteristic ratio of pure PAA at theta conditions[46]. The presence of GO appears to have only a minor effect as the temperature approaches the glass transition from above. The moderately smaller values in the composite within the glassy region is consistent with previous observations in a polymer/graphene nanocomposite, where it was found that this effect was related to a population of chain configurations bearing close end-to-end distances[47]. On average though, the shape of the polymer chains in the hybrid material (see figure S1 in the ESI) was found to be rather insensitive to the presence of the filler at the examined composition.

## 3.2. Polymer physical adsorption and local order close to the GO surface

As a first step towards exploring the characteristics of physical adsorption of PAA chains onto the GO sheets, we have examined the density profile of the polymer chains in a direction perpendicular to the GO plane. Since the shape of the GO does not remain perfectly planar after the equilibration procedure and during the production runs (see fig. 2), in consensus with previous works[44, 45], the effective definition of a GO plane was based on its center of mass and on the two principal axes of inertia of the platelet which were on average parallel to the GO surface. The direction of the third axis which completed the orthogonal system of the principal axes of inertia defined thus each flake's direction. The calculated density profiles are presented in figure 5. The zero value of the x-axis corresponds to the location of a GO plane as defined above.

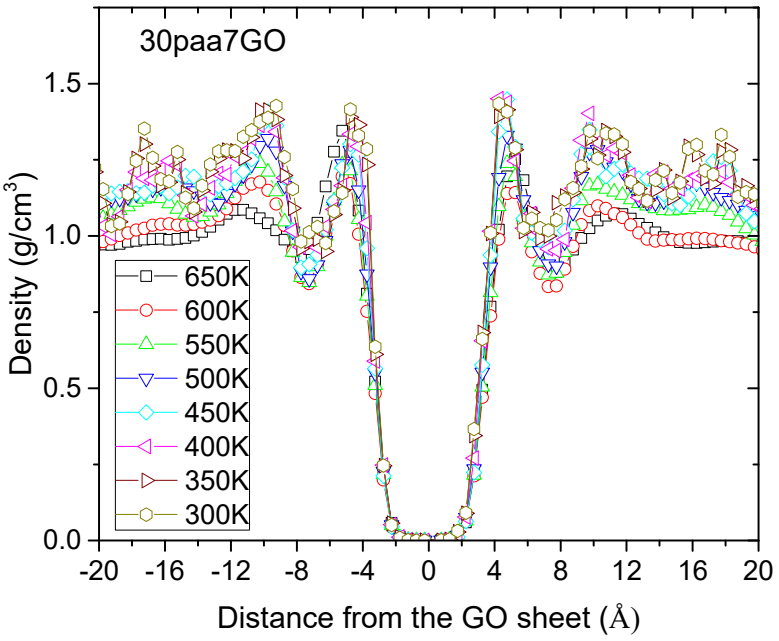


**Figure 5**: Density profiles of PAA along the direction perpendicular to a GO sheet

A key feature characterizing the profiles is the appearance of several peaks at different distances from a GO plane. This feature is close to the generic picture characterizing the density modulation of a linear polymer near a solid surface due to the packing constraints and the excluded volume effects[48] which is also present in the case where the solid surface is replaced by an atomic-thick sheet[49-51]. In the later studies where perfectly flat surfaces were examined, it was also found that the

intensity of the density peaks close to the surface assumed values 2-3 times higher compared to that of bulk polymer. In such cases, an anisotropy in the displacement of the adsorbed layer was also observed[52, 53]. This is clearly not the case in the composite system studied here. Our results, though, are consistent with the findings from a previous work where it was shown that the density profiles of adsorbed water on graphene changed (i.e., their intensity decreased) when the roughness of the surface increased[54]. On these accounts, this effect seems to be related to the non-flat surface of the GO used in our study.

Furthermore, in our system the corresponding substrate may consist either from a single or from multiple GO sheets as discussed earlier, so that the calculated spectra essentially reflect an overall average (i.e., irrespectively to whether a GO sheet belongs to a cluster or not). The first peak adjacent to the GO surface at a distance of 4 Å can be attributed to the physically adsorbed polymer layer, while the peaks at longer distances may also reflect those polymer segments that are located close to neighboring GO flakes, including those belonging in the same or in a neighboring cluster. A common characteristic of the observed peaks is that their intensity increases upon temperature decrease, which is consistent with a higher degree of monomer localization as the system enters the glassy state.

To check the orientation of the PAA monomers at different distances from a GO plane as the system approaches the glassy state from above, we have calculated the orientational parameter, $P_2$, of the backbone carbon-carbon (C-C) bonds (see schematic of the PAA monomer in figure 1) defined by

$$P_2(\phi) = \frac{1}{2}\left\langle 3\cos^2\phi - 1 \right\rangle \qquad (2)$$

In eq. 2, $\phi$ represents the angle between a PAA backbone C-C bond and the vector normal to a GO plane, as described earlier. The angle brackets indicate an ensemble and time average. $P_2(\phi)$ assumes a value equal to 1 for a parallel orientation of the two vectors, a value of -0.5 for a perpendicular arrangement and a value of 0 for a random orientation. The dependence of the bond orientational parameter on the distance from a GO plane and on the temperature is shown in figure 6. Visual inspection of the behavior of the C-C orientational parameter reveals that as the system enters the glassy region, a preferential orientation of the bonds normal to the

GO plane develops close to the GO surface. At the lowest examined temperature, almost half of the C-C bonds appear to arrange in this manner. This behavior differs from that observed in previous works[51, 55] where in polymer/graphene composite materials, a strong tendency for parallel orientation of the polymer backbone bonds was observed onto a perfectly flat graphene surface.

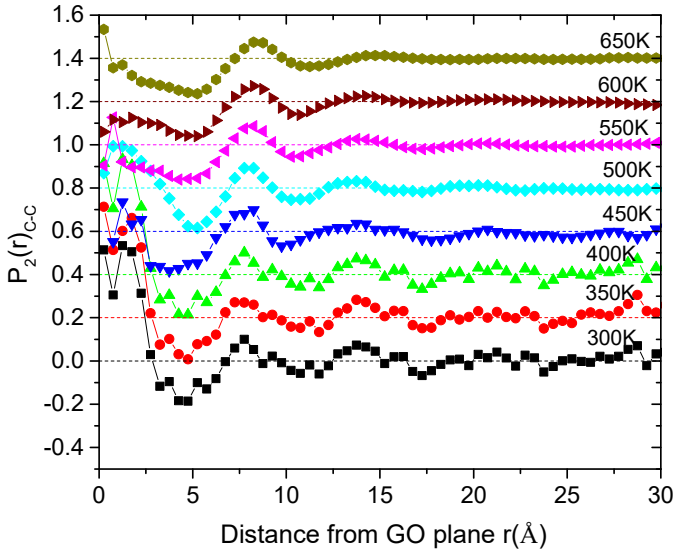


**Figure 6**: Polymer backbone C-C orientational parameter as a function of the distance from a GO plane for all the examined temperatures. Each curve is shifted on the y-axis by 0.2 with respect to its previous temperature. Dashed lines denote the corresponding zero levels.

To rationalize this picture, on one hand it must be taken into account that in our case the GO flakes are not perfectly flat, while on the other hand the presence of hydroxyls and epoxy oxygens onto the graphene's surface may impose certain geometric constraints which could hinder a parallel orientation of the PAA monomers close to a GO sheet. Moreover, the hydrogen-bonding-capable atomic pairs between PAA and GO may impel energetically favorable backbone arrangements other than parallel to the GO surface. Actually, in our case it is the hydroxyl hydrogen (HO) – hydroxyl oxygen (OH) bond of the PAA monomer that shows a tendency for a parallel to the GO plane orientation close to its surface (see figure S2 in ESI), which is enhanced as temperature drops.

## 3.3. PAA and PAA-GO hydrogen bonding

To explore the degree of intra and intermolecular hydrogen bonding between the polymer chains and GO, we have considered appropriate atomic pairs such as epoxy oxygens (OS)-hydroxyl hydrogens (HO) and hydroxyl oxygens (OH)-hydroxyl hydrogens (HO), between PAA molecules and GO and between PAA chains only. The definition of a hydrogen bond was based on geometric criteria, such as the hydrogen−oxygen distance and the angle θ formed by the donor−hydrogen−acceptor triplet. The minimum value for θ for the identification of the hydrogen bond was taken to be 120°.[56, 57]

To check the presence of hydrogen bonding within the potential donor-acceptor pairs, we have calculated the relevant pair correlation functions selecting only those pairs which satisfy the angle criterion described above. As an example figure 7 illustrates PAA HO-OH intra- and intermolecular pair correlation functions in the composite system.

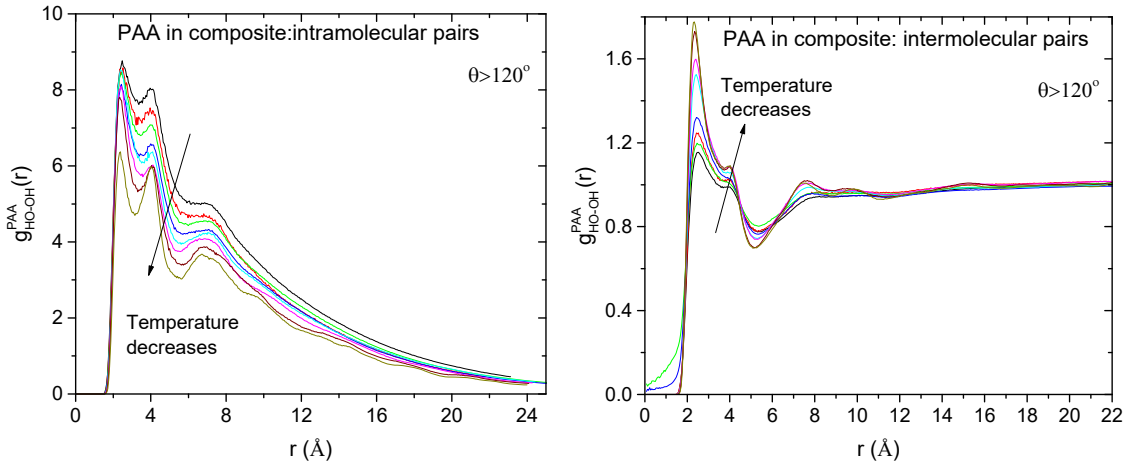


**Figure 7:** Pair correlation functions between hydroxyl hydrogens and hydroxyl oxygens for the PAA intramolecular (left) and the intermolecular (right) pairs in the composite system for all the examined temperatures.

In both cases a dominate peak appears close to a 2.5Å separation which is consistent with pairs forming a hydrogen bond[58]. The secondary peak in the intramolecular pairs can be attributed to the hydroxyl groups of the neighboring monomers. As shown in the corresponding intermolecular spectra, this peak is suppressed due to the lack of connectivity between the intermolecular pairs. The corresponding spectra in the pristine system are very similar (see fig. S3 in the ESI). Following the same procedure, we have calculated also the spectra for PAA-GO pairs as shown in figure 8. For both kinds of pairs examined, a hydrogen bonding peak (HBP) can be identified at a separation close to 2Å. The mere detection of hydrogen bonding in an

atomic pair, however, does not provide quantitative information as to the abundance and the longevity of the formed hydrogen bonds, which is important for the assessment of the degree of physical association between monomers belonging to the same chain or between two different molecules.

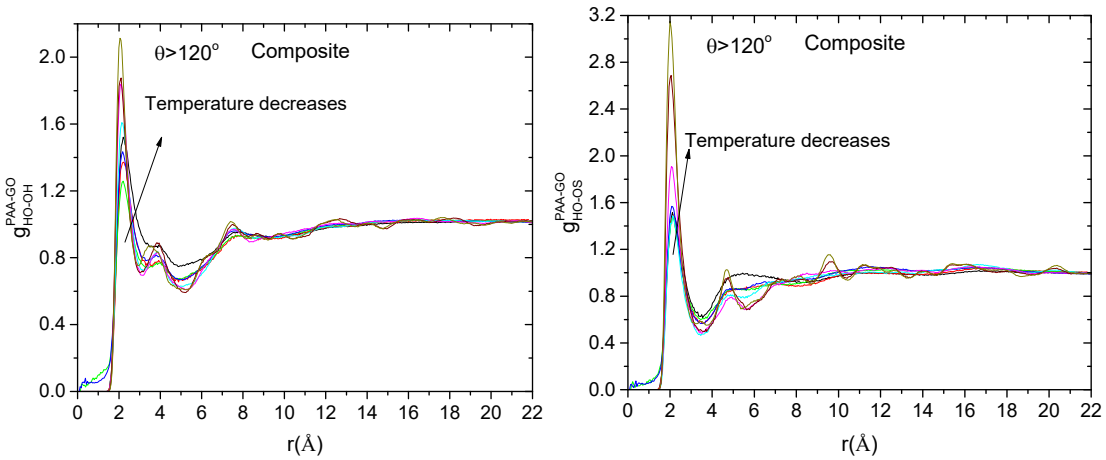


**Figure 8:** Inter-species pair correlation functions between hydroxyl hydrogens and hydroxyl oxygens (left) and between PAA hydroxyl hydrogens and GO epoxy oxygens (right) at all the examined temperatures.

For a more quantitative estimation we have measured the average number of hydrogen bonds, taking as maximum separation the extent of the HBP in the corresponding pair correlation functions. The result is presented in figure 9.

Focusing on the PAA HO-OH hydrogen-bonding behavior (fig. 9 left), it seems that there is a systematic (approximately linear) increase in the number of the interchain hydrogen bonds as temperature drops, both for chains in the pristine PAA system and in the composite. It appears that a significant percentage of PAA monomers per chain (varying between 20% and 30% approximately within the examined temperature range) participate in the interchain hydrogen bonding. The presence of GO imparts only a small decrease in the average number of interchain hydrogen bonds with respect to the pristine PAA system.

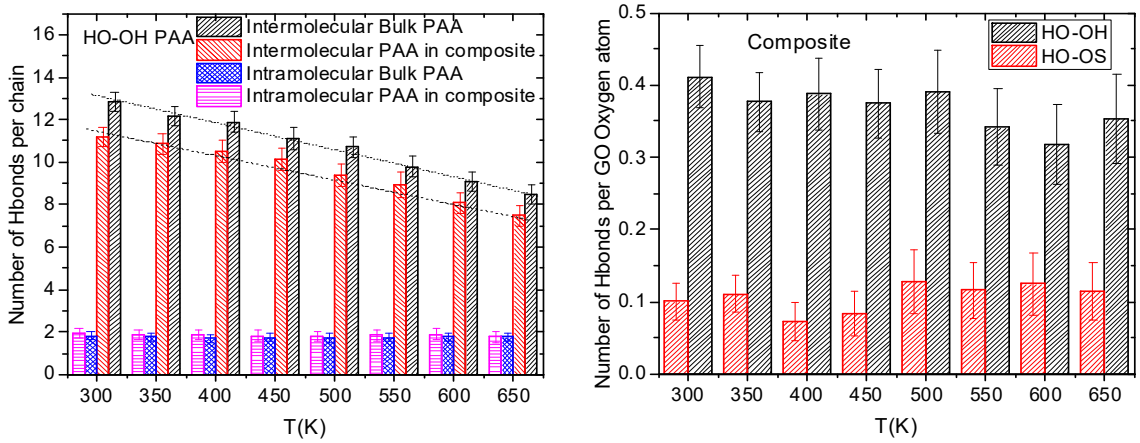

**Figure 9:** Average number of hydrogen bonds per timeframe. The left panel displays the average number of PAA intra- and intermolecular HO-OH hydrogen bonds per chain in the pristine polymer system and in the composite. The right panel shows the average number of inter-species HO-OH and HO-OS hydrogen bonds per GO oxygen atom. The lines in the left panel are guides to the eye.

On the contrary, the intrachain PAA hydrogen bonding remains practically unchanged as a function of temperature, while it does not seem to be affected by the presence of GO.

The enhancement of the degree of interchain hydrogen bonding in both systems can be rationalized by the increase in density as the temperature drops, which enhances the probability for hydrogen-bonding-capable atoms to form hydrogen bonds (i.e., due to the increase in the number of their atomic neighbors). In the case of the composite system, the GO intervention lowers to a certain extent the probability for interchain contacts, thus leading to a small decrease in the degree of the interchain hydrogen bonding. The apparent independence of the PAA intrachain hydrogen bonding to temperature, is consistent with the insensitivity observed in the chain shape characteristics (see fig. S1).

Looking at the PAA/GO hydrogen bonding (fig. 9 right) it is evident that the OH-OH pairs are much more frequent than those involving the GO epoxy oxygens. It appears also that there is no systematic dependence on temperature, for both examined pairs. To examine the longevity of the formed pairs, we have calculated the hydrogen bond correlation function[59] according to eq. 3

$$h(t) = \frac{\langle g(t)\, g(0) \rangle}{\langle g^2 \rangle} \qquad (3)$$

In this expression g(t)=1 for any examined pair, if this pair forms a hydrogen bond at time t, and 0 otherwise. Angle brackets denote averaging over all pairs and times. This function essentially expresses the probability of a hydrogen-bonded-capable pair being bonded at time t, provided that the pair formed a hydrogen bond at t=0. Because this function does not take into account any possible breaking in the interim time between t=0 and t, it is sensitive not to the lifetime of a bond remaining continuously intact, but rather to the long time behavior[60] which reflects the possibility of the atomic pair to remain in close vicinity and in an appropriate geometry in order to form a hydrogen bond. Spectra of h(t) for the HO-OH PAA/GO pair which is the more abundant is shown in figure 10.

It is clear that as the temperature lowers, the correlation functions decay at longer timescales. The short time regime at which all curves coincide, describes the very fast breaking and recombination process due to the librational motion of the bonds. The longer time regime where the curves differentiate strongly with temperature, should be associated with the slower change of the local environment as temperature drops.

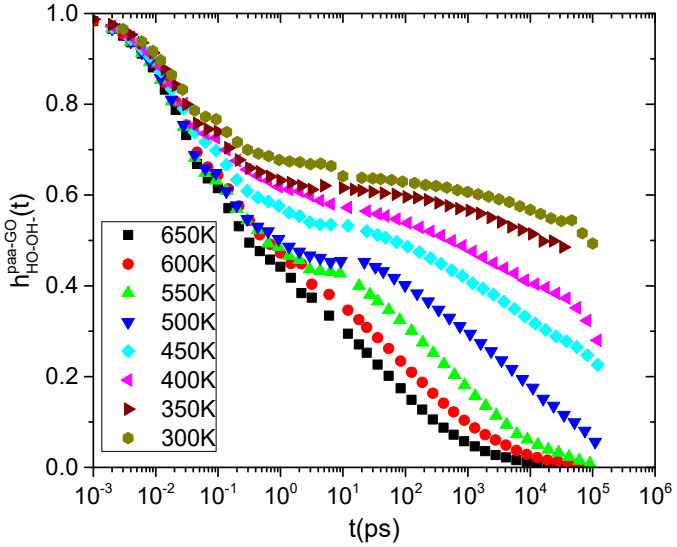


**Figure 10:** Hydrogen bond correlation functions for the HO-OH hydrogen bonding pair between PAA and GO, at the examined temperatures. Trajectories of shorter than 1fs timestep were generated for the calculation of the short time regime of the correlation functions.

To obtain an idea regarding the corresponding timescale, we have calculated a characteristic time $\tau_{1/e}$ at which $h(\tau_{1/e})=e^{-1}$. Figure 11 shows the dependence of the rates $\tau_{1/e}^{-1}$ extracted from the correlation functions of fig. 10 as a function of inverse temperature and compares them with those describing the dynamics of PAA/PAA pairs both, in the pristine polymer system and in the composite (see figure S4 in the ESI).

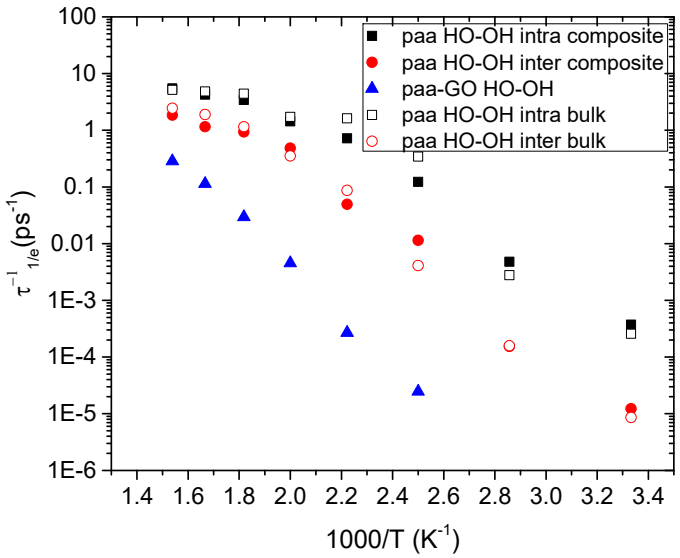

**Figure 11:** Relaxation rates vs inverse temperature for HO-OH pairs between PAA atoms and PA/GO atoms. In the legend description, "intra" corresponds to intermolecular and "inter" to intermolecular pairs.

Evidently, the HO-OH pairs formed between PAA and GO assume the lower rates, or in other words they correspond to the longer-lived hydrogen bonds. Due to the much stronger temperature dependence of the characteristic rate of the PAA/GO pairs compared to those of the PAA/PAA analogues, the time separation between the later and the former grows dramatically (reaching several orders of magnitude) as temperature decreases. Between the PAA/PAA HO-OH pairs, the intermolecular ones are somewhat longer-lived, while the presence of GO at the examined content does not appear to affect appreciably their characteristic timescale.

## 3.4 Effects of the presence of GO on polymer dynamics

To examine the effects of the presence of GO in polymer dynamics, we calculated appropriate time correlation functions probing motional processes at different lengthscales.

### 3.4.1 Effects in global polymer motion

To probe the overall rotational motion of the PAA chains, we monitored the second order correlation function of unit vectors $\hat{k}(t)$ connecting the center of mass of a polymer chain with its atoms according to eq 4

$$C_2(t) = \frac{1}{2}\left\langle 3\left[\hat{k}(t)\cdot\hat{k}(0)\right]^2 - 1\right\rangle \quad (4)$$

Angle brackets denote time and ensemble average over all vectors per chain and over all chains. Figure 12 presents $C_2(t)$ spectra describing the rotational motion of PAA chains in the pristine system and in the composite. As anticipated, all curves shift to longer timescales as temperature decreases. Moreover, at all temperatures shown, the correlation functions describing chain motion in the composite systems decay at longer timescales compared to those at the respective temperatures in the bulk. As these correlation functions reflect the average behavior considering all polymer

chains, it is reasonable to assume that this effect arises mostly by those chains in close vicinity to GO flakes, which may act as spatial obstacles to the chains' rotational diffusive motion.

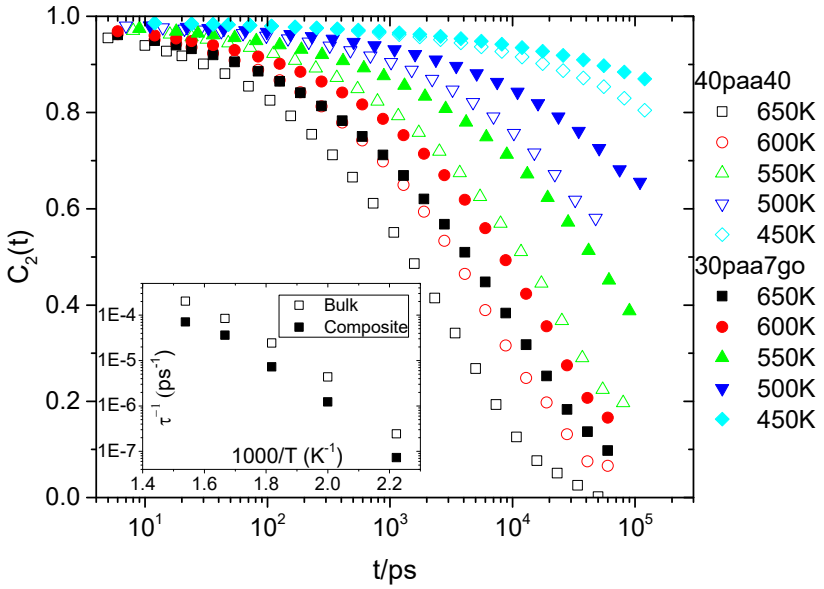


**Figure 12:** Overall rotational correlation functions for PAA chains in the pristine system (open symbols) and in the composite (filled symbols). The inset depicts the corresponding relaxation rates (see text) as a function of inverse temperature. Spectra at lower temperatures are not shown due to their very low degree of decorrelation in the examined time window.

To get an estimation of the relevant timescales exploiting also the behavior at lower temperatures where the degree of the decay of the correlation functions becomes very low, we have applied a method that mimics the time-temperature superposition principle employed in polymer rheology[61, 62]. Taking the correlation function of a temperature as reference (here 450K), we calculated the temperature shift factors necessary for the rest of the curves to superpose on a single mastercurve. Then, by estimating the absolute relaxation time at a temperature (here at 650K) where an adequate relaxation degree has been attained within our simulation window (i.e., by integrating the correlation function) and using the temperature shift factors, an estimation of the correlation times for the remaining curves was made.

The outcome of the superposition into a single mastercurve for the spectra shown in fig. 12, was excellent (see fig. S5 in the ESI) and the resulted relaxation rates are shown in the inset of fig. 12. The rates corresponding to the composite systems were found to be approximately 3 times lower compared to those in the pristine polymer. This finding can be understood if we take into account the physical adsorption of part of the chains onto the GO surface and the restricted diffusion of the rest of the chains

in the presence of the filler[63]. Namely, those PAA chains which become physically adsorbed onto a GO surface form polymer/GO complexes with increased effective mass and thus with a slower overall dynamics. On the other hand the GO flakes/clusters diffuse increasingly slower as temperature decreases, acting thus as a disordered array of slowly moving obstacles through which the non-adsorbed polymer chains must rearrange and diffuse[64, 65].

It is also noteworthy that the relaxation rates in both systems follow a similar temperature dependence, indicating that at temperatures above $T_g$ and in the examined GO content the relaxational mechanism for the overall chain motion remains the same in the bulk and in the composite. This notion does not necessarily remain true under conditions of a higher degree of constriction[47, 62].

### 3.4.1 Effects in local polymer motion

Dynamics in the length scale of a bond was examined by calculating rotational correlation functions (referred to as $g_2(t)$) using an expression analogous to eq 4, with the only difference that $\hat{k}(t)$ represented a unit vector along the examined bond. The $g_2(t)$ function essentially probes the rorientational motion of a bond, and its Fourier transform (i.e., the spectral density) is closely related to the outcome of Neutron Magnetic Resonance (NMR) experiments[66]. We focused on the dynamics of the backbone C-C and the hydroxyl HO-OH bonds of the PAA chain in the bulk and in the composite system, while we also examined in more detail the respective dynamic behavior close to the GO surface. Figure 13 depicts $g_2(t)$ spectra describing the dynamics of the C-C and the H-O vectors by taking into account all bonds of each kind.

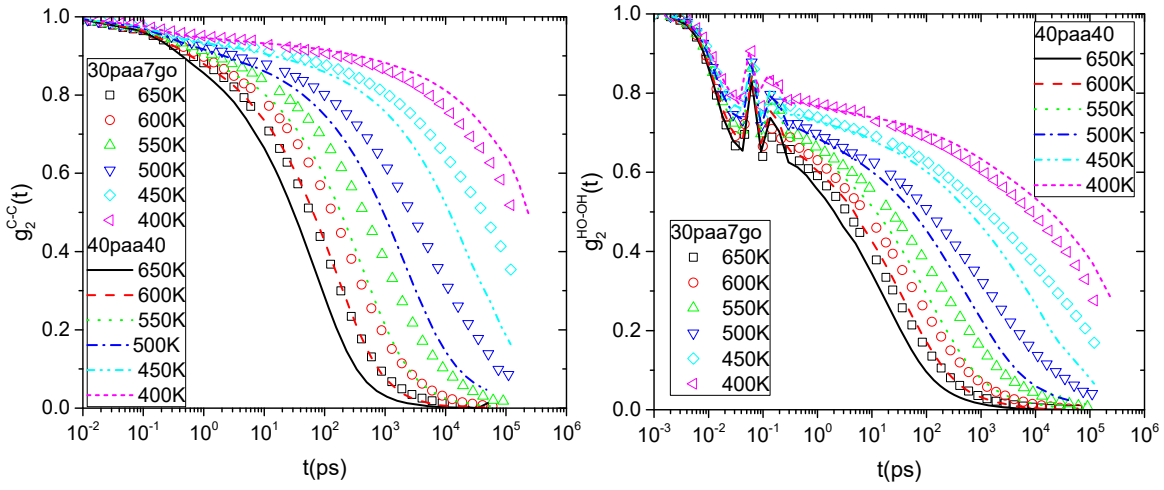

**Figure 13:** Reorientational correlation functions of the backbone C-C (left) and the hydroxyl HO-OH (right) bonds in the composite (symbols) and in the pristine PAA model (lines). Spectra at lower temperatures where the degree of decorrelation is quite low in the examined time range, are omitted for clarity. For the short time regime, trajectories with a timestep shorter than 1fs were produced.

These correlation functions reflecting an overall average of all bonds, describe dynamics which are usually accessible to experimental techniques such as dielectric spectroscopy, NMR and neutron scattering[66-68]. As shown in figure 13, in the regime above $T_g$ and for both kinds of bonds, for a specific temperature the decay of the correlation functions takes longer in the composite system. In addition, the C-C and the HO-OH spectra at the same temperature are characterized by distinct features.

The most striking difference is that the HO-OH curves show a peak at a timescale close to 0.1 ps which is absent from the C-C correlograms. This feature can be identified as a "recorrelation" in the bond rotational motion which is associated with the breaking and recombination of hydrogen bonds in which the HO-OH bonds participate[69]. A reasoning similar to that used for the overall chain rotational motion, can also be adopted in order to account for the somewhat slower timescale of the spectra describing the PAA bonds in the composite. A slower overall motion of chains near the GO surface can be reflected to bond dynamics as well[70, 71]. In addition, as was discussed in section 3.2, a higher density is observed close to a GO platelet, together with a considerable degree of bond ordering. Furthermore, the surface roughness of the GO sheets is expected to work towards retarding local dynamics with respect to the bulk[72]. All of these factors combined may contribute to the observed slowing down of bond reorientation near the GO moieties.

To quantify the degree of slowing down of bond motion in relation to its distance from a GO plane, we calculated $g_2(t)$ spectra of bonds located at different distance ranges from a GO sheet. Since the composite system was comprised by multiple GO platelets, we focused only on the two layers closer to a GO plane, in order to minimize the probability of "mixing" the dynamics between layers of different GO immediacy (e.g, a third layer of a GO sheet could also be the first layer of a neighboring GO plane). Figure 14 portrays $g_2(t)$ function for the backbone C-C and the HO-OH PAA bonds at a temperature above $T_g$, located within 0-4 Å (first layer) and 4-8 Å (second layer) from a GO plane and compares them with that describing the overall average (all distances included). Evidently, the layer closer to GO plane exhibits the lower degree of decorrelation (i.e., reflects slower dynamics). This layer

includes the bonds which are characterized by an enhanced local order and also participate in hydrogen bonding with the GO flakes (figures 6,7,8 and S2 in ESI). This dynamic differentiation of bonds adjacent to a GO flake is present at all the examined temperatures (see figure S6 in the ESI). It also persists for dynamic processes that require the synergistic motion of more than one bonds, such as the torsional transitions (see figure S7 in the ESI).

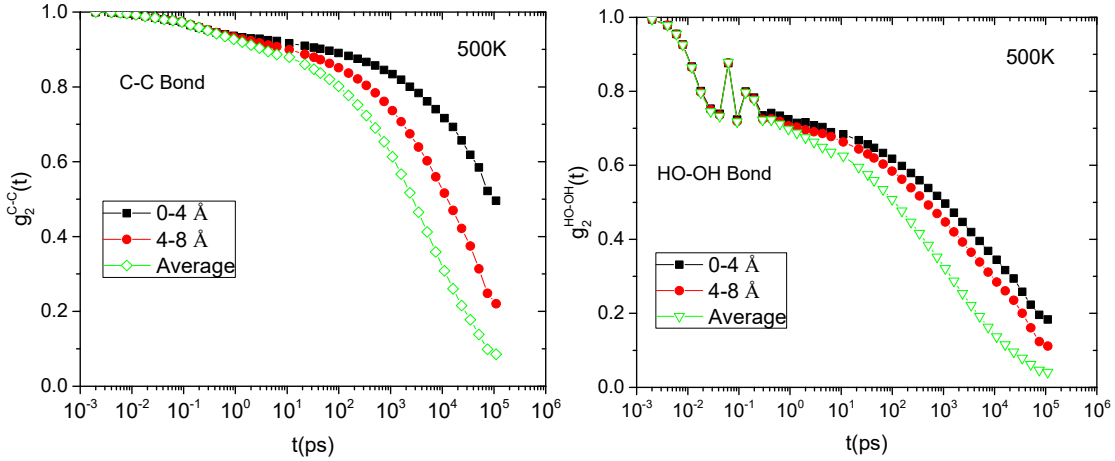


**Figure 14:** Reorientational correlation functions for C-C (left) and HO-OH (right) bonds at 500K for two layers adjacent to a GO plane (filled symbols) and for all the bonds (open symbols).

Figure 15 maps the relaxation rates $\tau_{1/e}^{-1}$ (following a definition as in section 3.2) resulted from spectra describing the reorientation of bonds belonging to the first and the second layers together with those corresponding to spectra describing the overall average.

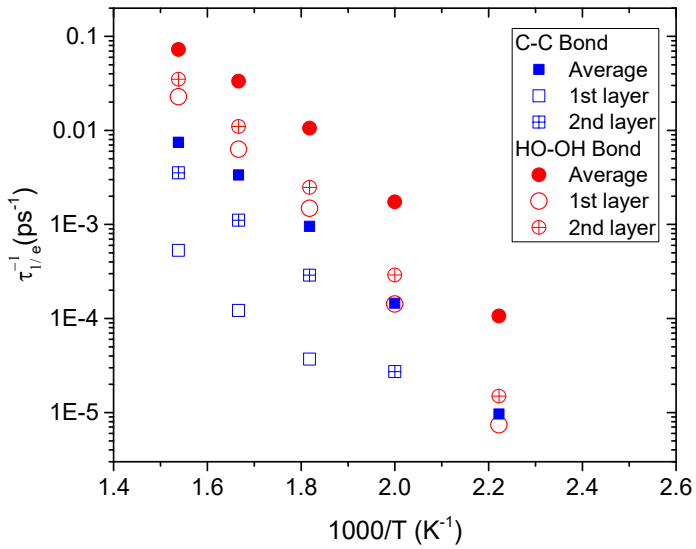


**Figure 15:** Reorientation relaxation rates for the C-C (squared symbols) and the HO-OH (circles) PAA bonds in the composite. Filled symbols represent the overall average, open symbols the 1st layer and crossed symbols the second layer.

The dependence of rates in figure 15 shows that the slowing down of bond reorientation at the first layer, with respect to the average behavior, amounts to a decade or larger particularly as temperature drops (while still in the region above the estimated $T_g$). This slowing down is considerably larger (approximately twice as high) for the C-C bonds when compared to the retardation experienced by the HO-OH analogues. Although to a first approximation it might have been expected that formation of hydrogen bonds between PAA and GO close to the GO surface could have resulted to a more severe retardation of the HO-OH bonds, this did not come to be the case since the relevant hydrogen bonding survival times were found to be much smaller (i.e., corresponded to much higher rates) than the times required for the HO-OH reorientation, even at the layer immediately adjacent to GO. Actually, hydrogen bonding between the polymer and GO could increase the hindrance for polymer backbone rearrangements, thus contributing further to the slowing down of the reorientation of the backbone bonds close to the GO surface.

## 3.5 Conclusions

In this study we have employed fully atomistic molecular dynamics simulations in order to examine in detail a nanocomposite material comprised by graphene oxide and poly(acrylic acid) in the absence of solvent.

The dispersion of the GO flakes in the polymer matrix was characterized by the formation of oligomeric clusters in coexistence with isolated GO sheets. The presence of GO shifted the apparent glass transition of the mixture to a higher temperature compared to the pristine polymer system, in line with previous experimental studies in graphene/polymer composites[44]. This effect can be directly correlated to the overall average slowing down at a local length scale (i,e. that of a bond or few bonds) as can be recorded by relevant experimental methods, which is known to be related to the so-called α-relaxation that drives a polymer-based system to the glass transition[73].

This apparent average dynamic slowing down, was found to originate mainly by the behavior of monomers immediately adjacent to a GO flake, with the bonds belonging to the polymer backbone (C-C) assuming a slower mobility compared to those in side groups (HO-OH), despite the possible participation of the latter in hydrogen bonding. Only part of the bonds belonging to such monomers were found to adopt an ordered

arrangement, resulting in rather low intensity peaks in the density profile normal to the rough GO surface. The orientational relaxation of these bonds was realized in the presence of a GO/PAA hydrogen bonds mostly involving hydroxyl groups. The latter were found to be significantly longer lived and with a stronger temperature dependence in their dynamics, compared to analogous intra and intermolecular hydrogen bonds involving only polymer chains. The number of the PAA/PAA hydrogen bonds was found to decrease in the presence of GO.

Dynamics on the lengthscale of the entire chain in the composite was also found to be slower compared to that in the pristine PAA system, but following a similar temperature dependence. As the chain-wide rotational motion of pure PAA was found to be time-temperature superposable, it appears that the implied rheological simplicity of the pure polymer remains present also in the mixture with GO at the examined content.

The system examined in the present work bears some intriguing features, such as the nanoscale dimensions of the GO flakes in polymer dispersions which recently came into focus[16, 74-76] and the hydrogen bonding between the graphene-based filler and the polymer matrix. It also elucidates effects of the GO surface roughness in the polymer adsorption profile and in local polymer dynamics at the GO/polymer interface. Such features are expected to be present in a broader range of composite materials formed by components with similar physicochemical attributes and thus may offer the basis for the interpretation of some key aspects of their physical behavior.

*Electronic supplementary information (ESI) available*: Shape parameters of polymer chains, orientational parameter of the HO-OH bond of the PAA monomer with respect to the GO plane, OH-OH pair correlation functions in the PAA pristine system, hydrogen bond correlation functions for the PAA HO-OH pairs, mastercurves and shift factors for the overall chain correlation functions, comparison between the spectra describing reorientational dynamics of bonds belonging to the 1st layer close to a GO plane and the corresponding overall average, comparison of torsional autocorrelation spectra at different distance ranges from a GO plane to those describing the average behavior of all the dihedrals.

**Notes and references**


1. L. Zhao, H. Sun, N. Kim, J. Lee, Y. Kong and P. Li, *J. Appl. Polym. Sci.*, 2015, **132**, 41973.
2. A. A. Gokhale, J. Lu, N. J. Parker, A. P. Izbicki, O. Sanyal and I. Lee, *J. Colloid Interf. Sci.*, 2013, **409**, 219-226.
3. J.-T. Chen, Y.-J. Fu, Q.-F. An, S.-C. Lo, S.-H. Huang, W.-S. Hung, C.-C. Hu, K.-R. Lee and J.-Y. Lai, *Nanoscale*, 2013, **5**, 9081-9088.
4. G. Hazell, M. Hinojosa-Navarro, T. M. McCoy, R. F. Tabor and J. Eastoe, *J. Colloid Interf. Sci.*, 2016, **464**, 285-290.
5. C. Gao and G. Chen, *Compos. Sci. Technol*, 2016, **124**, 52-70.
6. Z. Zhiheng, F. R. Georgia, M. Qingshi, Z. Shenmin, K. Hsu-Chiang and M. Jun, *Nanotechnology*, 2016, **27**, 042001.
7. M. M. Hasani-Sadrabadi, N. Mokarram, M. Azami, E. Dashtimoghadam, F. S. Majedi and K. I. Jacob, *Polymer*, 2011, **52**, 1286-1296.
8. W. Sun, T. Peng, Y. Liu, S. Xu, J. Yuan, S. Guo and X.-Z. Zhao, *J. Mater. Chem. A*, 2013, **1**, 2762-2768.
9. J. Zheng, X. Ma, X. He, M. Gao and G. Li, *Procedia Engineering*, 2012, **27**, 1478-1487.
10. D. Priftis, *Curr. Org. Chem.*, 2015, **19**, 1819-1827.
11. E. De Giglio, D. Cafagna, M. A. Ricci, L. Sabbatini, S. Cometa, C. Ferretti and M. Mattioli-Belmonte, *J. Bioact. Compat. Pol.* , 2010, **25**, 374-391.
12. J. Shen, B. Yan, T. Li, Y. Long, N. Li and M. Ye, *Soft Matter*, 2012, **8**, 1831-1836.
13. Z. Tai, J. Yang, Y. Qi, X. Yan and Q. Xue, *RSC Adv.*, 2013, **3**, 12751-12757.
14. V. K. Thakur and M. K. Thakur, *Chemical Functionalization of Carbon Nanomaterials: Chemistry and Applications*, CRC Press 2015.
15. J. E. Glass, ed., *Water-Soluble Polymers*, American Chemical Society, 1983.
16. E. K. Goharshadi, G. Akhlamadi and S. J. Mahdizadeh, *RSC Adv.*, 2015, **5**, 106421-106430.
17. D. Konios, M. M. Stylianakis, E. Stratakis and E. Kymakis, *J. Colloid Interf. Sci.*, 2014, **430**, 108-112.
18. M. Zhong, Y.-T. Liu and X.-M. Xie, *J. Mater. Chem. B*, 2015, **3**, 4001-4008.
19. J. Zhang, M. S. Azam, C. Shi, J. Huang, B. Yan, Q. Liu and H. Zeng, *RSC Adv.*, 2015, **5**, 32272-32282.
20. C. Cheng, Z. Liu, X. Li, B. Su, T. Zhou and C. Zhao, *RSC Adv.*, 2014, **4**, 42346-42357.
21. C. Liu, X. Liu, H. Xuan, J. Ren and L. Ge, *Sci. Rep.-UK*, 2015, **5**.
22. M. Xu, J. Zhu, F. Wang, Y. Xiong, Y. Wu, Q. Wang, J. Weng, Z. Zhang, W. Chen and S. Liu, *ACS Nano*, 2016, **10**, 3267-3281.
23. V. Mittal, ed., *Polymer-Graphene Nanocomposites*, The Royal Society of Chemistry, 2012.
24. P. Mukhopadhyay and R. K. Gupta, eds., *Graphite, Graphene, and their polymer nanocomposites*, CRC Press, 2013.
25. D. Stauffer, N. Dragneva, W. B. Floriano, R. C. Mawhinney, G. Fanchini, S. French and O. Rubel, *J. Chem. Phys.*, 2014, **141**.
26. A. Bagri, C. Mattevi, M. Acik, Y. J. Chabal, M. Chhowalla and V. B. Shenoy, *Nat Chem*, 2010, **2**, 581-587.

27. W. D. Cornell, P. Cieplak, C. I. Bayly, I. R. Gould, K. M. Merz, D. M. Ferguson, D. C. Spellmeyer, T. Fox, J. W. Caldwell and P. A. Kollman, *J. Am. Chem. Soc.*, 1995, **117**, 5179-5197.
28. D. J. Sparks, M. E. Romero-Gonzalez, E. El-Taboni, C. L. Freeman, S. A. Hall, G. Kakonyi, L. Swanson, S. A. Banwart and J. H. Harding, *Phys. Chem. Chem. Phys.*, 2015, **17**, 27357-27365.
29. Z. Adamczyk, A. Bratek, B. Jachimska, T. Jasinski and P. Warszynski, *J Phys Chem B*, 2006, **110**, 22426-22435.
30. J. Wang, R. M. Wolf, J. W. Caldwell, P. A. Kollman and D. A. Case, *J. Comput. Chem.*, 2004, **25**, 1157-1174.
31. J. Wang, W. Wang, P. A. Kollman and D. A. Case, *J. Mol. Graph. Model.*, 2006 **25**, 247260.
32. L. Martínez, R. Andrade, E. G. Birgin and J. M. Martínez, *J. Comput. Chem.*, 2009, **30**, 2157-2164.
33. S. E. Feller, Y. Zhang, R. W. Pastor and B. R. Brooks, *J. Chem. Phys.*, 1995, **103**, 4613-4621.
34. T. Darden, L. Perera, L. Li and L. Pedersen, *Structure*, 1999, **7**, R55-R60.
35. J. Phillips, R. Braun, W. Wang, J. Gumbart , E. Tajkhorshid, E. Villa, C. Chipot, R. Skeel, L. Kale and K. Schulten, *J. Comput. Chem.* , 2005, **26**, 1781–1782.
36. L. Gong, R. J. Young, I. A. Kinloch, I. Riaz, R. Jalil and K. S. Novoselov, *ACS Nano*, 2012, **6**, 2086-2095.
37. R. J. Young, I. A. Kinloch, L. Gong and K. S. Novoselov, *Compos. Sci. Technol.*, 2012, **72**, 1459-1476.
38. C. Sung, A. Vidyasagar, K. Hearn and J. L. Lutkenhaus, *Langmuir*, 2012, **28**, 8100-8109.
39. W. Paul, in *Reviews in Computational Chemistry*, John Wiley & Sons, Inc., 2007, DOI: 10.1002/9780470189078.ch1, pp. 1-66.
40. G. Kritikos, *Polymer*, 2014, **55**, 4658-4670.
41. I. C. Sanchez and R. H. Lacombe, *J. Phys. Chem. C*, 1976 **80**, 2352–2362.
42. L. Shao and J. L. Lutkenhaus, *Soft Matter*, 2010, **6**, 3363-3369.
43. T. Lucyshyn, G. Knapp, M. Kipperer and C. Holzer, *J. Appl. Polymer Sci.*, 2012, **123**, 1162-1168.
44. RamanathanT, A. A. Abdala, StankovichS, D. A. Dikin, M. Herrera Alonso, R. D. Piner, D. H. Adamson, H. C. Schniepp, ChenX, R. S. Ruoff, S. T. Nguyen, I. A. Aksay, R. K. Prud'Homme and L. C. Brinson, *Nat. Nano.*, 2008, **3**, 327-331.
45. Q. Xue, C. Lv, M. Shan, H. Zhang, C. Ling, X. Zhou and Z. Jiao, *Comp. Mater. Sci.*, 2013, **71**, 66-71.
46. L. F. Gudeman and N. A. Peppas, *J. Appl. Polym. Sci.*, 1995, **55**, 919-928.
47. R.-E. Roussou and K. Karatasos, *Mater. Design*, 2016, **97**, 163-174
48. J. Baschnagel and K. Binder, *Macromolecules*, 1995, **28**, 6808-6818.
49. A. N. Rissanou and V. Harmandaris, *Soft Matter*, 2014, **10**, 2876-2888.
50. Y. Gao, J. Liu, L. Zhang and D. Cao, *Macromol. Theor. Simul.*, 2013, **23**, 36-48.
51. A. Rissanou and V. Harmandaris, *J. Nanopart. Res.*, 2013, **15**, 1-14.
52. G. Kritikos, A. Sgouros, G. G. Vogiatzis and D. N. Theodorou, *J. Phys. Conf. Ser.*, 2016, **738**, 012012.
53. G. Kritikos and A. F. Terzis, *Eur. Polym. J.*, 2013, **49**, 613-629.

54. J. Marti and M. C. Gordillo, *J. Phys. Chem. B*, 2010, **114**, 4583-4589.
55. A. N. Rissanou, A. J. Power and V. Harmandaris, *Polymers*, 2015, **7**, 390-417.
56. E. Chiessi, F. Cavalieri and G. Paradossi, *J. Phys. Chem. B*, 2007, **111**, 2820-2827.
57. G. A. Jeffrey and W. Saenger, *Hydrogen Bonding in Biological Structures*, Springer-Verlag, Berlin, 1991.
58. J. C. Speakman, *The hydrogen bond and other intermolecular forces*, The Chemical Society, London, 1975.
59. D. C. Rapaport, *Mol. Phys.*, 1983, **50**, 1151 - 1162.
60. F. W. Starr, J. K. Nielsen and H. E. Stanley, *Phys. Rev. Lett.*, 1999, **82**, 2294-2297.
61. G. Strobl, *The Physics of Polymers*, Springer Berlin, 3rd edn., 2007.
62. K. Karatasos, *Macromolecules*, 2014, **47**, 8833-8845.
63. S. V. Larin, S. G. Falkovich, V. M. Nazarychev, A. A. Gurtovenko, A. V. Lyulin and S. V. Lyulin, *RSC Adv.*, 2014, **4**, 830-844.
64. O. A. Hickey and G. W. Slater, *Phys Lett A*, 2007, **364**, 448-452.
65. W.-S. Tung, N. Clarke, R. J. Composto and K. I. Winey, *Macromolecules*, 2013, **46**, 2317-2322.
66. K. Karatasos, J. P. Ryckaert, R. Ricciardi and F. Lauprêtre, *Macromolecules*, 2002, **35**, 1451-1462.
67. F. Barroso-Bujans, S. Cerveny, A. Alegria and J. Colmenero, *Macromolecules*, 2013, **46**, 7932-7939.
68. F. Barroso-Bujans, F. Fernandez-Alonso, S. Cerveny, S. F. Parker, A. Alegria and J. Colmenero, *Soft Matter*, 2011, **7**, 7173-7176.
69. I. Tanis, D. Tragoudaras, K. Karatasos and S. H. Anastasiadis, *J. Phys. Chem. B*, 2009, **113**, 5356-5368.
70. K. Karatasos and D. B. Adolf, *J. Chem. Phys.*, 2000, **112**, 8225-8228.
71. H. Morhenn, S. Busch, H. Meyer, D. Richter, W. Petry and T. Unruh, *Phys. Rev. Lett.*, 2013, **111**, 173003.
72. P. Scheidler, W. Kob and K. Binder, *EPL (Europhysics Letters)*, 2002, **59**, 701.
73. R.-J. Roe, in *Atomistic Modeling of Physical Properties*, eds. L. Monnerie and U. W. Suter, Springer Berlin Heidelberg, Berlin, Heidelberg, 1994, DOI: 10.1007/BFb0080198, pp. 111-144.
74. J. Zou and F. Kim, *Nat. Commun.*, 2014, **5**.
75. J. Xin, R. Zhang and W. Hou, *J. Mater. Chem. B*, 2014, **2**, 3697-3704.
76. S. Guo and S. Dong, *Chem. Soc. Rev.*, 2011, **40**, 2644-2672.